Luminescence Concentration Quenching Mechanism in Gd2O3:Eu(3+)

ARTICLE *in* THE JOURNAL OF PHYSICAL CHEMISTRY A · FEBRUARY 2014

Impact Factor: 2.69 · DOI: 10.1021/jp4119502 · Source: PubMed

6 AUTHORS, INCLUDING:

Octavio Meza Espinoza
Meritorious Autonomous University of Puebla
23 PUBLICATIONS **155** CITATIONS
SEE PROFILE

Edgar Giovanny Villabona Leal
Meritorious Autonomous University of Puebla
3 PUBLICATIONS **23** CITATIONS
SEE PROFILE

Luis Armando Diaz-Torres
Centro de Investigaciones en Optica
103 PUBLICATIONS **1,111** CITATIONS
SEE PROFILE

Elías Pérez
Universidad Autónoma de San Luis Potosí
79 PUBLICATIONS **546** CITATIONS
SEE PROFILE

THE JOURNAL OF PHYSICAL CHEMISTRY A

Article

pubs.acs.org/JPCA

Luminescence Concentration Quenching Mechanism in $Gd_2O_3:Eu^{3+}$.

Octavio Meza,*[,†] E. G. Villabona-Leal,[†,‡] L. A Diaz-Torres,[§] H. Desirena,[§] J. L. Rodríguez-López,[∥] and Elías Pérez[⊥]

[†]Instituto de Física "Ing. Luis Rivera Terrazas", Benemérita Universidad Autónoma de Puebla, Apartado Postal J-48, Puebla 72570, México

[‡]Posgrado en Ciencias Aplicadas, Facultad de Ciencias, Universidad Autónoma de San Luis Potosí, Av. Salvador Nava, 078290 San Luis Potosí, México

[§]Grupo de Espectroscopia de Materiales Avanzados y Nanoestructurados (EMANA), Centro de Investigaciones en Óptica, A. P.1-948, Gto, 37150 León, México

[∥]División de Materiales Avanzados, Instituto Potosino de Investigación Científica y Tecnológica, A.C., Camino Presa San José, Lomas 4ª Secc, 78216 San Luis Potosí, México

[⊥]Instituto de Física, Universidad Autónoma de San Luis Potosí, Álvaro Obregón #64, 78000 San Luis Potosí, México

ABSTRACT: Luminescence concentration quenching in $Gd_2O_3:Eu^{3+}$ nanocrystals results from strong interactions among O^{2-} ions and Eu^{3+} ions. Because all synthesized $Gd_2O_3:Eu^{3+}$ nanocrystals present the same cubic crystalline phase regardless of Eu^{3+} concentration, it is possible to study the optical properties as a function of the dopant concentration. The emission intensities and lifetime curves for $Gd_2O_3:Eu^{3+}$ were analyzed by a simple rate equation model to study the interaction between the O^{2-} ions and Eu^{3+} ions. The rate equation model considers that such interaction is driven by the following energy transfer processes: the direct energy transfer ($O^{2-} \rightarrow Eu^{3+}$), back-transfer ($Eu^{3+} \rightarrow O^{2-}$), and direct energy migration ($Eu^{3+} \rightarrow Eu^{3+}$). The exact solution of this model agrees with the experimental results, luminescence concentration quenching is reproduced and the corresponding energy transfer rates are reported. Quantitative results suggest that the direct energy transfer and direct energy migration processes are the main responsible for the luminescence concentration quenching, whereas the back-transfer process promotes the Eu^{3+} emission.

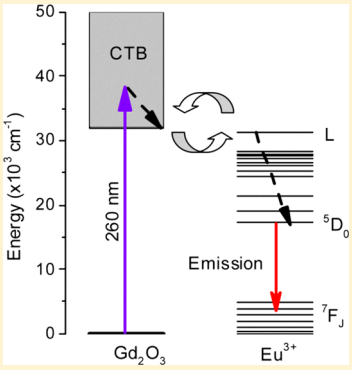

1. INTRODUCTION

In recent years, there is great interest in the generation of visible light sources for a variety of application purposes, such as solid-state multicolor three-dimensional displays, detection of biomolecules,[1,2] white-light generation and two-photon confocal microscopy.[3,4] Rare earth compounds have been widely used as high-performance luminescent devices, catalysts, and other functional materials based on the electronic, optical, and chemical characteristics arising from 4f electrons. Furthermore, rare earth ions hosted in phosphorus exhibit unique optical properties such as long fluorescence lifetime, single to multicolor emission, infrared to visible up-conversion luminescence, large Stokes shift and good luminescence efficiency combined with high photochemical stability of the hosts.[5]

As is known, the phonon energy[6] of the Gd_2O_3 matrix is about 600 cm^{-1}, which is much lower than for Al_2O_3 (870 cm^{-1}) and SiO_2 (1100 cm^{-1}) but higher than that of Y_2O_3 (300−380 cm^{-1}). Thus, Gd_2O_3 is an appropriate host for the development of highly luminescent materials because it is chemically and photochemically stable, besides it has also a high refractive index. Indeed, the most important Gd_2O_3 crystalline phase in technological applications is the cubic phase, which can be obtained in the temperature range from 600 to 1200 °C. Furthermore, it is well-known that the substitution of rare earth (RE) ions into the Gd^{3+} does not change the cubic crystalline phase, and that the lattice parameter depends almost exclusively on the processing temperature.[7,8]

In the present work, we present a simple model, based on a particular system of ordinary differential equations for to study the interaction between the O^{2-} ions and Eu^{3+} ions. This interaction leads to a broad absorption band that might be identified as the well-known charge transfer band (CTB). The nonradiative and radiative relaxation constants, as well as a quantitative estimation of the energy transfer processes among Eu^{3+} and O^{2-} ions are reported for the $Gd_2O_3:Eu^{3+}$ system.

2. EXPERIMENTAL DETAILS

2.1. Synthesis of $Gd_2O_3:Eu^{3+}$ Nanophosphorus.

$Gd_2O_3:Eu^{3+}$ powders were synthesized and characterized as follows: *X* mol of $Eu(NO_3)_3{\cdot}6H_2O$ and *Y* mol of $Gd(NO_3)_3{\cdot}6H_2O$ were added to 40 mL of ethylene glycol (99.8%, Sigma-Aldrich, Mexico) under vigorous stirring. Then 20 mL of H_2O (18 MΩ) was added, followed by 1 g of polyethylene glycol

Received: December 5, 2013
Revised: February 8, 2014
Published: February 11, 2014

   dx.doi.org/10.1021/jp4119502 | *J. Phys. Chem. A* 2014, 118, 1390−1396

10000 (Sigma-Aldrich, Mexico). The resulting mixture was heated at 50 °C under stirring until homogeneity was achieved, and then 40 mL of 1 M sodium hydroxide was added. Immediately after such addition, Gd^{3+} and Eu^{3+} hydroxide crystals started to form, and the solution was aged for 15 min under continuous stirring. The product was then transferred to a stainless steel autoclave with a Teflon inner coating and brought to 200 °C for 24 h. Upon completion of the time, the system was removed and kept at room temperature. The resulting white solid precipitate is then washed with water and ethanol several times. Then the product was allowed to dry at 70 °C for 12 h and annealed at 1000 °C for 3 h. The Eu^{3+} ion concentration in the matrix was varied by performing a scan of concentration from a minimum of 0.1 to a maximum of 7.0%, an additional sample with no Europium ions was prepared. Composition calculations were made on mole percent, as shown in the following relationship: $Eu^{3+}:Gd^{3+} = X:(1 - X)$ and $X + Y = 1$, where X is the molar fraction of Eu^{3+} and Y is the mole fraction of Gd^{3+}.

2.2. Crystalline Structure and Morphology. The crystalline phase of the nanocrystals was determined by X-ray powder diffraction using a Bruker AXS D8 Advance diffractometer with a Cu tube with Ka radiation at 1.5405 Å, scanning in the 20−110° 2θ range with increments of 0.02° and a swept time of 1 s. In addition, the morphology of the samples was analyzed through a Helios Nanolab 600 Dual-Beam scanning electron microscope (SEM).

2.3. Optical Characterization. Samples were subjected to heat treatment prior to optical characterization. They were heated to 80 °C for 4 h and later were introduced into a desiccator for 12 h. Excitation and emission spectrum were obtained by a Varian Cary Eclipse fluorescence spectrophotometer. The pump excitation (at 260 nm) was modulated by a chopper at 100 MHz to obtain the lifetime curves in 612 nm band emission.

3. RESULTS AND DISCUSSION

3.1. Structural and Morphological Characterization. Figure 1 shows the diffraction spectra for undoped and doped $Gd_2O_3:Eu^{3+}$ nanophosphors, all samples have the same cubic structure (space group $Ia\bar{3}$ and JCPDS 65-3181). XRD patterns do not show evidence of any other phases or impurities. This suggests dopant ions are dispersed uniformly in the matrix and

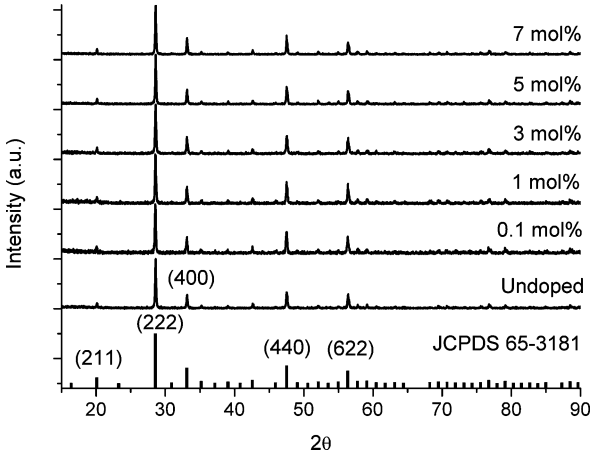

Figure 1. Diffraction spectra for undoped and doped $Gd_2O_3:Eu^{3+}$ nanophosphors. All the samples have the same cubic structure.

native ions are being replaced effectively.[9] It is important to emphasize that crystalline phase plays an important role for the probability of radiative versus nonradiative decay mechanisms;[10,11] this is mainly due to the fact that the energy transfer processes are highly dependent on the interionic distances and crystalline symmetry properties. Because all samples present the same phase, it is possible to study the optical properties as a function of the dopant concentration. Figure 2 shows the SEM images for 0.1, 3.0, 7.0, and 10 mol %

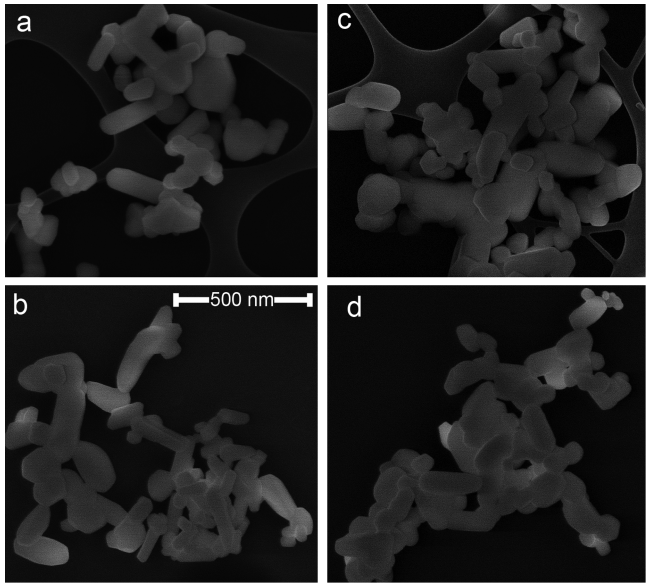

Figure 2. SEM images for (a) 0.1, (b) 3.0, (c) 7.0, and (d) 10 mol % of Eu^{3+} concentration. All images have the same scale. There was no significant difference in morphology as a function of dopant concentration.

of Eu^{3+} concentration, all the samples have a variety of shapes with average sizes around 123 ± 71 nm, and there was no significant difference on morphology as a function of all dopant concentration.

3.2. Luminescence Properties of $Gd_2O_3:Eu^{3+}$ Powders. The excitation spectra were measured by observing the maximum emission at 612 nm, which correspond to the $^7F_2 \rightarrow {}^5D_0$ transition. Emission spectra were measured in the range from 525 to 725 nm at an excitation wavelength of 260 nm. Both excitation and emission spectra are shown in Figure 3. Excitation spectra for all samples present a wide excitation band around 230 and 260 nm that corresponds to the charge transfer band (CTB) transitions and is attributed to O^{2-} (2p) → Eu^{3+} (4f) ligand-to-metal charge transfer.[12] Another excitation peaks correspond to f−f transitions. Emission spectra were carried out by exciting the CTB at 260 nm. All samples show the characteristic Eu^{3+} emissions from the $^5D_0 \rightarrow {}^7F_j$ transitions, where j runs from 0 to 4 and $^5D_1 \rightarrow {}^7F_i$, where i is 1 or 2. The signals at 537, 553, 565, 587, 612, 651, and 708 nm correspond to the transitions $^5D_1 \rightarrow {}^7F_1$, $^5D_1 \rightarrow {}^7F_2$, $^5D_0 \rightarrow {}^7F_0$, $^5D_0 \rightarrow {}^7F_1$, $^5D_0 \rightarrow {}^7F_2$, $^5D_0 \rightarrow {}^7F_3$ and $^5D_0 \rightarrow {}^7F_4$, respectively.[13,14] The states $^5D_0 \rightarrow {}^7F_1$ and $^5D_0 \rightarrow {}^7F_3$ are magnetic dipole transitions independent of the chemical environment surrounding the active ion. The strongest signal emission corresponds to the hypersensitive electric dipole allowed by the transition $^5D_0 \rightarrow {}^7F_2$. This transition is present only when the Eu^{3+} ions are located in inversion center sites within the crystalline lattice. It

dx.doi.org/10.1021/jp4119502 | J. Phys. Chem. A 2014, 118, 1390−1396

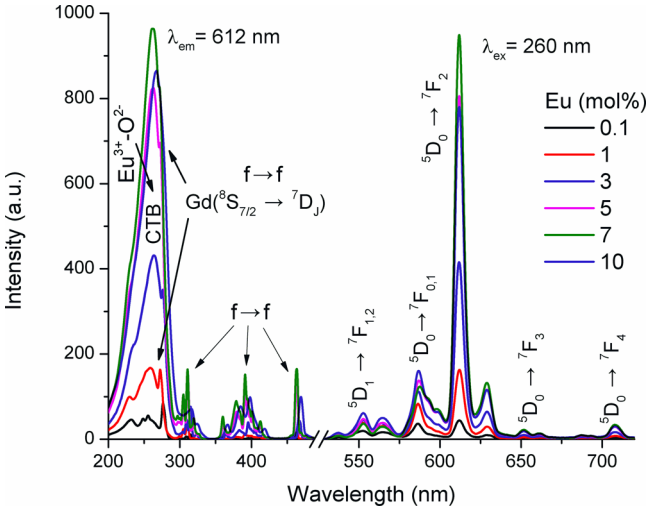

Figure 3. Excitation (left) and emission (right) spectra of Gd_2O_3:Eu^{3+}.

is well-known that a cubic lattice has Gd_2O_3 as the two types of sites[15] available for insertion of rare earth ions, and such sites have point symmetry groups C_2 and S_6. These sites are in a ratio of 3 C_2 to each S_6. Eu^{3+} ions located at S_6 sites within the crystal lattice of Gd_2O_3 possess inversion center,[16] favoring transitions $^5D_0 \rightarrow {}^7F_{0,1}$. Furthermore, Eu^{3+} ions are located at the C_2 sites, which do not possess inversion center symmetry, making it possible to observe emission from the electric dipole forced transitions $^5D_0 \rightarrow {}^7F_{2,4}$.

Emission intensity depends strongly on dopant concentration as can be observed in emission spectra in Figure 3. To quantify this dependence, Figure 4 shows the integral of the

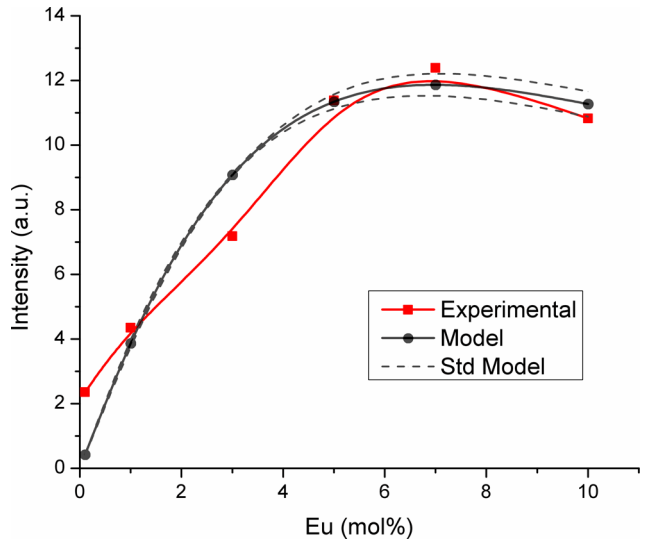

Figure 4. Integral of the emission spectrum from 525 to 725 nm vs Eu^{3+} concentration; experimental, theoretical results, and confidence interval of the model.

emission spectra (φ) from 525 to 725 nm, plotted as function of Eu^{3+} concentration. This emission range corresponds to the $^5D_0 \rightarrow {}^7F_j$ transitions and is directly proportional to the population in $^5D_0$ energy level.[11,15−17] It is observed that φ increases as Eu^{3+} concentration increases from 0.1 to 7.0 mol %. Then for higher concentrations there is a decrease in φ as Eu^{3+} concentration increases up to 7.0 mol % (Figure 4). The luminescent dynamics of the $^5D_0$ energy level can be estimated using the lifetime curves. Decay lifetime curves in Figure 5

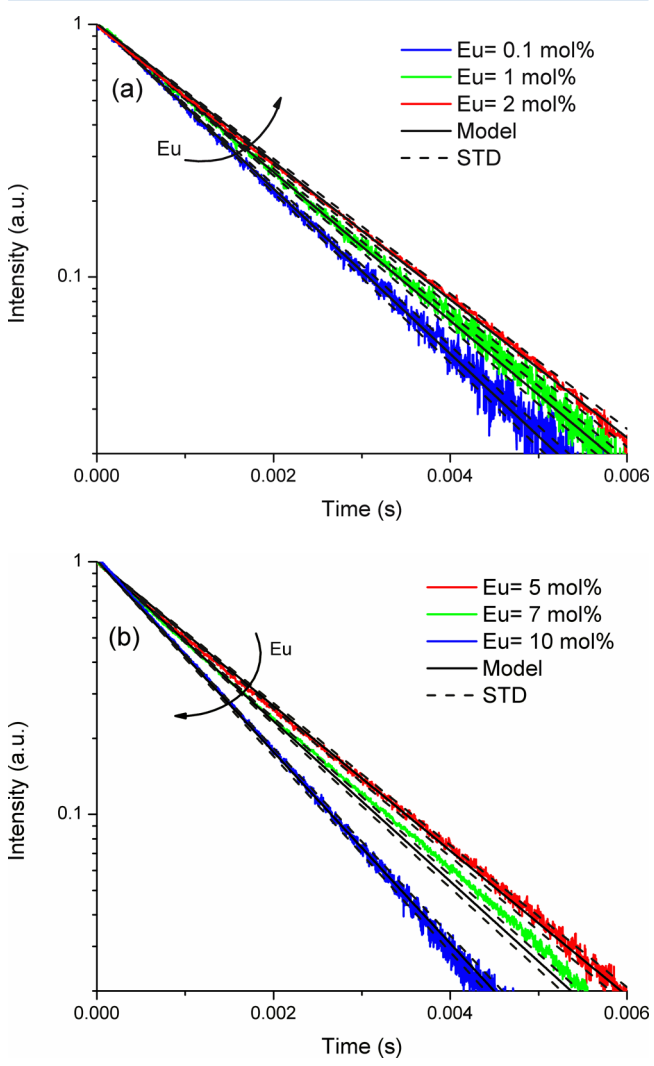

Figure 5. Experimental and theoretical lifetime curves. The resuts shows two opposite behaviors: (a) the slope of the curve decreases with Eu^{3+} concentration and (b) the slope of the curve increases with the dopant concentration.

shows two opposite concentration dependence behaviors: (a) the slope of the curve decreases with Eu^{3+} concentration and (b) the slope of the curve increases with the dopant concentration. Thus, the lifetime curves depend on dopant concentration. To quantify the effect of dopant concentration on the luminescent dynamics, we estimate the effective lifetime (τ_{eff}) by adjusting the experimental curves with a single exponential function, $\exp(-t/\tau_{eff})$. Figure 6 shows τ_{eff} as a function of the dopant concentration. For concentrations less than 3 mol %, the τ_{eff} increases with dopant concentration. On the other hand, a decrease in τ_{eff} is observed for higher concentrations. It is also important to emphasize that emission intensity (φ) and effective lifetime are the most important parameters for luminescent materials; both experimental properties are summarized in the Table 1. One of the traditional tools for studying the emission intensity and effective lifetime is the rate equations models.

3.3. Rate Equation Model. The Figure 7 shows schematically the energy levels diagram of Gd_2O_3:Eu^{3+} and the simplest

dx.doi.org/10.1021/jp4119502 | J. Phys. Chem. A 2014, 118, 1390−1396

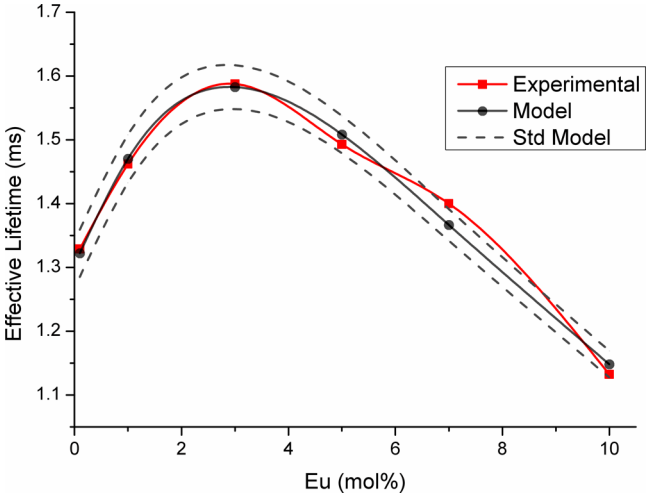

Figure 6. Experimental and theoretical effective lifetimes as a function of the concentration of Eu^{3+} ions.

Table 1. Eu^{3+} Concentration, Population in the Ground State, Eu−Eu Interionic Distance, Experimental Effective Lifetime, and Emission Intensity

Eu^{3+} (mol %)	P^0_{Eu} (ions/cm^3)	r (Å)	τ_{eff} (ms)	Φ (au)
0.1	2.35×10^{19}	34.9	1.33	2.4
1	2.35×10^{20}	16.2	1.46	4.3
3	7.05×10^{20}	11.2	1.59	7.2
5	1.18×10^{21}	9.5	1.49	11.4
7	1.65×10^{21}	8.5	1.40	12.4
10	2.36×10^{21}	7.5	1.13	10.8

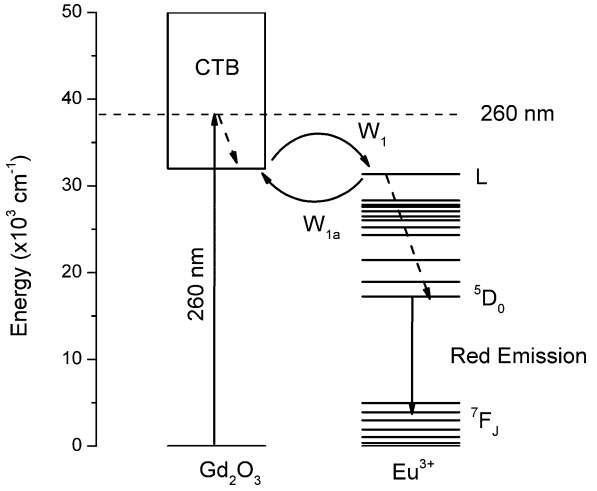

Figure 7. Energy diagram displaying the proposed relaxation mechanism for the luminescence emission.

energy transfer mechanism to generate red emission under 260 nm pumping. First, some ions on ground state are excited to CTB due to lamp pumping (260 nm); after that, some of the following phenomena may occur: nonradiative transition of O^{2-} ions described by relaxation rates A_{CTB} (s^{-1}), or a phonon-assisted direct energy transfer W_1 (cm^3/s) that represent the transitions related to $O^{2-} \rightarrow Eu^{3+}$. Once some Eu^{3+} ions are excited on the level L, the following mechanisms or processes can take place: phonon-assisted back-transfer W_{1a} (cm^3/s), $Eu^{3+} \rightarrow O^{2-}$, or a fast nonradiative relaxation from upper Eu^{3+} level L to the lower $^5D_0$ energy level. Then, when the Eu^{3+} ions are in $^5D_0$ energy level, the following two processes can take place: (a) nonradiative and radiative relaxation $^5D_0 \rightarrow {}^7F_j$ ($j = \{0, ..., 6\}$), described by the overall relaxation rate A_{Eu} (s^{-1}), or (b) a cross relaxation ($^5D_0$, ^7F_j) → (^7F_j, $^5D_0$) between Eu^{3+} ions, W_2 (cm^3/s). The mechanisms described above can be expressed by the following rate equation model:[18]

$$\frac{dP^1_{Eu}(t)}{dt} = -(A_{Eu} + W_{1a}P^0_{CTB} + W_2P^0_{Eu})P^1_{Eu} + W_1P^0_{Eu}P^1_{CTB} \quad (1)$$

$$\frac{dP^1_{CTB}(t)}{dt} = -(A_{CTB} + W_1P^0_{Eu})P^1_{CTB} + W_{1a}P^0_{CTB}P^1_{Eu} \quad (2)$$

where P^1_{Eu} and P^1_{CTB} are the population densities of the excited Eu^{3+} and O^{2-} states and P^0_{Eu} and P^0_{CTB} are the population densities of the ground states. Furthermore, taking into account (for low pump lamp intensity or low absorption cross section) that the excited-state populations are a small fraction of the overall population of Eu^3 and O^{2-} states, it can be assumed that P^0_{Eu} and P^0_{CTB} are proportional to the nominal concentrations. The initial conditions described in the diagram of Figure 7 are $P^1_{Eu}(0) = 0$ and $P^1_{CTB}(0) \neq 0$, and this is because Eu^{3+} ions are not resonant with the pumping (260 nm). In this case, the solution for the excited population of Eu^{3+} ions is

$$P^1_{Eu}(t) = P^1_{CTB}(0)\frac{W_1P^0_{Eu}}{\beta}(\exp(-t/\tau^s_1) - \exp(-t/\tau^s_2)) \quad (3)$$

where

$$\beta = (Q_1{}^2 - 2Q_1Q_2 + Q_2{}^2 + 4W_1P^0_{Eu}W_{1a}P^0_{CTB})^{1/2} \quad (4)$$

$$\tau^s_{1,2} = \left(\frac{Q_1 + Q_2 \mp \beta}{2}\right)^{-1} \quad (5)$$

$$Q_1 = A_{Eu} + W_{1a}P^0_{CTB} + W_2P^0_{Eu} \quad (6)$$

$$Q_2 = A_{CTB} + W_1P^0_{Eu} \quad (7)$$

Equation 3 has two terms $\tau^s_{1,2}$, where τ^s_1 is the lifetime and τ^s_2 is the rise time. Thus, τ^s_1 must be equal to experimental lifetime τ_{eff}. On the other hand, to estimate the integrated emission intensity (Figure 4), we need to solve the rate equation in stationary conditions, because the emission spectra (Figure 3) were measured under such stationary conditions, unlike of the lifetime curves (Figure 5). In the latter case it is necessary to add the absorption pump rate (R) into eq 2 (see the Appendix). Then, the solution for P^1_{Eu} in the stationary condition considering the absorption pump in the eq 2 follows

$$P^1_{Eu} = \frac{RP^0_{Eu}W_1}{Q_1Q_2 - P^0_{CTB}P^0_{Eu}W_1W_{1a}} \quad (8)$$

Taking into account the absorption pump rate equation, for low incident pump power the emission intensity depends linearly on incident pump power.[19,20] On the other hand, the Eu^{3+} population on $^5D_0$ energy level is proportional to emission intensity on the $^5D_0 \rightarrow {}^7F_j$ transitions, i.e., $\varphi = kP^1_{Eu}$. Where k is a constant that depends on experimental equipment and it is the same for all the samples. To find the constant parameters of the Gd_2O_3:Eu^{3+} luminescence dynamics, we define the following function

dx.doi.org/10.1021/jp4119502 | J. Phys. Chem. A 2014, 118, 1390−1396

$$f = \sum_{i=\mathrm{Eu}} [(\tau^{s}_{1,i} - \tau_{\mathrm{eff},i})^2/\tau_{\mathrm{eff},i} + (kP^{1}_{\mathrm{Eu}} - \varphi)^2/\varphi] \quad (9)$$

To find the minimum of eq 9, we use the trust-region-reflective optimization method and 50 random initial conditions. The trust-region-reflective algorithm is a subspace trust-region method and is based on the interior-reflective Newton method.[21,22] These 50 random initial conditions conduce to 50 possible solutions to eq 9, i.e., 50 lifetimes curves (eq 3) and 50 emission intensity predictions (eq 8). Whereby the mean and standard deviation values from relaxations and transfer rates are equal to $A_{\mathrm{Eu}} = 213 \pm 30$ (s^{-1}), $A_{\mathrm{CTB}} = 767 \pm 3$ (s^{-1}), $W_1 = (205 \pm 45) \times 10^8$ ($cm^3\ s^{-1}\ N_a^{-1}$), $W_2 = (181 \pm 10) \times 10^3$ ($cm^3\ s^{-1}\ N_a^{-1}$), $W_{1a}P^0_{\mathrm{CTB}} = (362 \pm 84) \times 10^5$ (s^{-1}), $kR = (144 \pm 1) \times 10^2$ (au) and N_a is the Avogadro number. It is important to emphasize that energy transfer depend on the dopant concentration and nature of the electric, magnetic and/or exchange interaction,[19,23] this complicates the analytical solution of the rate equation model, for simplicity, we consider the energy transfer as a constant for all dopant concentrations. Figure 4 shows the experimental emission intensity and the mean model prediction. As can be seen there, the experimental tendency and concentration quenching are reproduced by the simple theoretical prediction. To estimate de energy transfer fraction of each energy transfer process on the luminescent dynamics, we define the following relations:

$$T(\mathrm{O}^{2-}\rightarrow\mathrm{Eu}^{3+}) = \frac{P^0_{\mathrm{Eu}}W_1}{P^0_{\mathrm{Eu}}W_1 + P^0_{\mathrm{Eu}}W_2 + P^0_{\mathrm{CTB}}W_{1a}} \quad (10)$$

$$T(\mathrm{Eu}^{3+}\rightarrow\mathrm{Eu}^{3+}) = \frac{P^0_{\mathrm{Eu}}W_1}{P^0_{\mathrm{Eu}}W_1 + P^0_{\mathrm{Eu}}W_2 + P^0_{\mathrm{CTB}}W_{1a}} \quad (11)$$

$$T(\mathrm{Eu}^{3+}\rightarrow\mathrm{O}^{2-}) = \frac{P^0_{\mathrm{CTB}}W_{1a}}{P^0_{\mathrm{Eu}}W_1 + P^0_{\mathrm{Eu}}W_2 + P^0_{\mathrm{CTB}}W_{1a}} \quad (12)$$

$T(\mathrm{O}^{2-}\rightarrow\mathrm{Eu}^{3+})$ is related with direct energy transfer between the CTB band to Eu^{3+} ions, $T(\mathrm{Eu}^{3+}\rightarrow\mathrm{Eu}^{3+})$ is related with direct energy migration of the excitation along a chain of Eu^{3+} ions, and typically this is one of the most important mechanisms for luminescence concentration quenching. Finally, $T(\mathrm{Eu}^{3+}\rightarrow\mathrm{O}^{2-})$ is the back-transfer between Eu^{3+} ions to O^{2-}, in this process Eu^{3+} ions feedback the CTB band. Figure 8 shows the plot for the eqs 10−12 vs Eu^{3+} concentration. To be able to observe the $T(\mathrm{Eu}^{3+}\rightarrow\mathrm{Eu}^{3+})$ effect, eq 11 has been multiplied by 10^4. Thus, for concentrations below to 4.6 mol % the dominant energy transfer process is $Eu^{3+} \rightarrow O^{2-}$. In this case, Eu^{3+} ions feedback the CTB band holding the luminescence. For concentrations greater than 4.6 mol %, the dominant energy transfer process is $O^{2-} \rightarrow Eu^{3+}$. For this case, primarily the CTB band is depopulated and the feedback process is less important, i.e., the luminescence concentration quenching occurs. Figures 4 and 5 show these two regimes: (i) for lower dopant concentration to 4.6 mol %, the emission intensity increase rapidly (Figure 4) and lifetimes curves (Figure 5a) are shifted to longer τ_{eff} when the dopant concentration increases; on the other hand (ii) for upper dopant concentration to 4.6 mol %, the inhibition of luminescence is observable and the lifetimes curves have a τ_{eff} decrement (Figure 5b). Another important aspect shown in Figure 8 is that $Eu^{3+} \rightarrow Eu^{3+}$ energy transfer effect is very small compared with the $Eu^{3+} \rightarrow O^{2-}$ and $O^{2-} \rightarrow Eu^{3+}$ energy transfer effects. However, the $Eu^{3+} \rightarrow Eu^{3+}$ effect is necessary in our model to reproduce the experimental results, specially the concentration quenching effect. To find the effect of the $W_2(\mathrm{Eu}^{3+}\rightarrow\mathrm{Eu}^{3+})$ effect on luminescence concentration quenching, we find ground-state population for Eu^{3+} ions to have the maximum emission value of the eq 8:

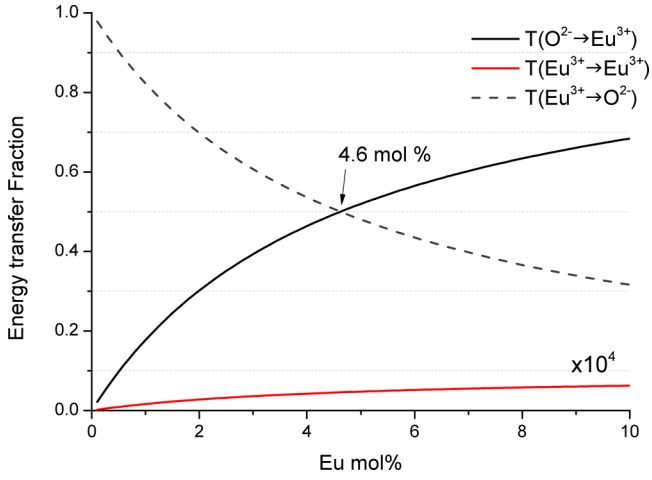

Figure 8. Energy transfer effect. To observe the $T(\mathrm{Eu}^{3+}\rightarrow\mathrm{Eu}^{3+})$ effect, we multiplied by 10^4. For concentrations below to 4.6 mol %, the dominant energy transfer process is $Eu^{3+} \rightarrow O^{2-}$. For concentrations greater than 4.6 mol %, the dominant energy transfer process is dictated by $O^{2-} \rightarrow Eu^{3+}$.

$$P^0_{\mathrm{Eu,max}} = \left(\frac{A_{\mathrm{CTB}}(A_{\mathrm{Eu}} + W_{1a}P^0_{\mathrm{CTB}})}{W_1W_2}\right)^{1/2} \quad (13)$$

Substituting the relaxations and transfer rates values into eq 13, we find the optimal Eu^{3+} concentration to have the maximum emission intensity, 7 mol %. Also, the eq 13 shows that $W_1(\mathrm{O}^{2-}\rightarrow \mathrm{Eu}^{3+})$ and $W_2(\mathrm{Eu}^{3+}\rightarrow \mathrm{Eu}^{3+})$ play a fundamental role in the luminescence concentration quenching effect. In the limit as W_1 or W_2 approaches to cero, the Eu^{3+} concentration tends to infinity to have luminescence concentration quenching. Thereby, it is demonstrated that both W_1 and W_2 play a role in the luminescence concentration quenching as a function of dopant concentration. The eq 13 has been experimentally estimated by other authors.[24−27] Table 2 shows the required concentration to reach the maximum emission intensity and the corresponding Eu−Eu interionic distance (see the Appendix) for different oxides: TiO_2, Gd_2O_3, Y_2O_3, and ZrO_2. It is important to emphasize that experimental estimation of Chih-Cheng Lin[25] fits with our prediction to have the maximum emission intensity (7 mol %) for the same host. Averaging the mean interionic distances for the TiO_2, Gd_2O_3, Y_2O_3, and ZrO_2 materials, we find that it is equal to 8.1 ± 1.0 Å. This mean interionic distance is the optimal configuration to have the optimum emission intensity for the samples reported.

Table 2. Concentration To Have the Maximum Emission Intensity and Eu−Eu Interionic Distance for Several Hosts

material	Eu^{3+} (mol %)	P^0_{Eu} (Ions/cm^3)	r (Å)	ref
TiO_2:Eu	10	2.47×10^{21}	7.4	24
Gd_2O_3:Eu	7	1.65×10^{21}	8.5	25
Y_2O_3:Eu	5	1.22×10^{21}	9.3	26
ZrO_2:Eu	10	2.69×10^{21}	7.2	27
Gd_2O_3:Eu	7	1.65×10^{21}	8.5	this work

dx.doi.org/10.1021/jp4119502 | J. Phys. Chem. A 2014, 118, 1390−1396

4. CONCLUSIONS

The emission intensities and lifetime curves for Gd_2O_3:Eu^{3+} for several dopant concentrations were analyzed by a simple rate equation model. The exact solution of this model agrees with the experimental results; furthermore, luminescence concentration quenching is reproduced. Results suggest two dominant energy transfer mechanisms and its magnitudes of interaction depend on dopant concentration in two regimens: (i) for concentrations below to 4.6 the dominant energy transfer process is $Eu^{3+} \rightarrow O^{2-}$ (in this case, Eu^{3+} ions feedback the CTB band holding the luminescence), and (ii) for concentrations greater than 4.6 the dominant energy transfer process is $O^{2-} \rightarrow Eu^{3+}$ (for this case, primarily the CTB band is depopulated and the feedback less important; i.e., the luminescence concentration quenching occurs). Additionally, although $Eu^{3+} \rightarrow Eu^{3+}$ energy migration of the excitation effect is very small compared with $Eu^{3+} \rightarrow O^{2-}$ and $O^{2-} \rightarrow Eu^{3+}$ energy transfer effects, the $Eu^{3+} \rightarrow Eu^{3+}$ effect is necessary in our model to reproduce the experimental results, in particular the concentration quenching effect.

APPENDIX

Assuming the density of Gd_2O_3 is a constant, the population of the P^0_{Eu} (ions/cm^3) is related with the concentration for low pumping power by

$$P^0_{Eu} \approx \frac{2X\left(\frac{W}{MW}\right)N_a}{V} \tag{A.1}$$

where X is the mole fraction of Eu^{3+} ions (X = mol %/100), N_a is the Avogadro number, V is the volume in cm^3, W is the weight of sample, and MW is molecular weight of Gd_2O_3:Eu^{3+}. Recall that the density (ρ) is equal to W/V and MW can be rewritten as

$$MW = 2(MW_{Gd}(1 - X) + MW_{Eu}X) + 3MW_O \tag{A.2}$$

where MW_{Gd}, MW_{Eu}, and MW_O are the molecular weight of Gd, Eu, and O elements, respectively. Thereby, the population on ground state (ions/cm^3) for Eu^{3+} ions is

$$P^0_{Eu} \approx \frac{2X\rho N_a}{2(MW_{Gd}(1 - X) + MW_{Eu}X) + 3MW_O} \tag{A.3}$$

The Eu−Eu interionic distance is generally proportional to[19,28]

$$r = (P^0_{Eu})^{-1/3} \tag{A.4}$$

Absorption Pump Rate

The absorption pump rate is the probability per unit time that atom absorbs photon, and the absorption pump rate R is given by[5]

$$R = \frac{\lambda_p}{hc\pi w_p^2} P\sigma P^0_{CTB} \tag{A.5}$$

where P is the incident pump power, λ_p is the pump wavelength, w_p is the pump radius, h is Planck's constant, c is the vacuum speed of light, and σ is the absorption cross section.

Maximum Emission Value

The emission intensity in the stationary condition is equal to

$$P^1_{Eu} = \frac{RP^0_{Eu}W_1}{Q_1Q_2 - P^0_{CTB}P^0_{Eu}W_1W_{1a}} \tag{A.6}$$

To find the optimal Eu^{3+} concentration to have the maximum emission intensity, we need to solve the following equation

$$\frac{dP^1_{Eu}}{dP^0_{Eu}} = 0 \tag{A.7}$$

Solving eq A.7 for the ground-state population for Eu^{3+} ions, we find that

$$P^0_{Eu,max} = \left(\frac{A_{CTB}(A_{Eu} + W_{1a}P^0_{CTB})}{W_1W_2}\right)^{1/2} \tag{A.8}$$

AUTHOR INFORMATION

Corresponding Author

*O. meza: e-mail, omeza@ifuap.buap.mx.

Notes

The authors declare no competing financial interest.

ACKNOWLEDGMENTS

The authors thank to Central Laboratory at IFUAP, for providing access to its facilities, and the CONACYT grant number 167939.

REFERENCES

(1) Khorasani-Motlagh, M.; Noroozifar, M.; Niroomand, S.; Moodi, A. Photoluminescence Studies of a Terbium(III) Complex as a Fluorescent Probe for DNA Detection. *J. Lumin.* **2013**, *143*, 56−62.

(2) Gonga, L.; Maa, M.; Xua, C.; Lia, X.; Wangc, S.; Lina, J.; Yanga, Q. Multicolor Upconversion Emission of Dispersed Ultrasmall Cubic Sr_2LuF_7 Nanocrystals Synthesized by a Solvothermal Process. *J. Lumin.* **2013**, *134*, 718−723.

(3) Schrofa, W.; Becka, E.; Etzrodta, G.; Hintze-Brüningb, H.; Meisenburgb, U.; Schwalma, R.; Warming, J. Depth-Resolved Characterization of UV Cured Coatings by Confocal Raman and Two-Photon Microscopy. *Prog. Org. Coat.* **2001**, *43*, 1−9.

(4) Desirena, H.; De la Rosa, E.; Salas, P.; Meza, O. Red, Green, Blue and White Light Upconversion Emission in Yb^{3+}/Tm^{3+}/Ho^{3+} Codoped Tellurite Glasses. *J. Phys. D: Appl. Phys.* **2011**, *44*, 1−4.

(5) Yersin, H. Transition Metal and Rare Earth Compounds: Excited States, Transitions, Interactions II, (Berlín). *Ed. Springer* **2001**, *214*, 1−56.

(6) Xiao, H.; Li, P.; Jia, F.; Zhang, L. General Nonaqueous Sol-Gel Synthesis of Nanostructured Sm_2O_3, Gd_2O_3, Dy_2O_3, and Gd_2O_3:Eu^{3+} Phosphor. *J. Phys. Chem. C* **2009**, *113*, 21034−21041.

(7) Chaa, B. K.; Muralidharanb, P.; Leeb, S. J.; Kimb, D. K.; Choc, G.; Jeona, S.; Huha, Y. Hydrothermal Synthesis, Structure and Scintillation Characterization of Nanocrystalline Eu^{3+}-Doped Gd_2O_3 Materials and Its X-Ray Imaging Applications. *Nucl. Instrum. Methods A* **2011**, *652*, 212−215.

(8) Pavitra, E.; Yu, J. S. A Facile Large-Scale Synthesis and Luminescence Properties of Gd_2O_3:Eu^{3+}. *Nanoflowers Mater. Lett.* **2013**, *90*, 134−137.

(9) Bazzia, R.; Floresa, M. A.; et al. Synthesis and Properties of Europium-Based Phosphors on the Nanometer Scale: Eu_2O_3, Gd_2O_3:Eu, and Y_2O_3:Eu. *J. Colloid Interface Sci.* **2004**, *273*, 191−197.

(10) Buijs, M.; Blasse, G. Energy Migration in a Two-Dimensional Eu^{3+} Compound: $EuMgAl_{11}O_{19}$. *J. Solid. State. Chem.* **1987**, *71*, 296−304.

(11) Meza, O.; Diaz-Torres, L. A.; Salas, P.; De la Rosa, E.; Solis, D. Color Tunability of The Upconversion Emission in Er−Yb Doped the Wide Band Gap Nanophosphors ZrO_2 and Y_2O_3. *Mater. Sci. Eng. B* **2010**, *174*, 177−181.

(12) Dhananjaya, N.; Nagabhushana, H.; Nagabhushana, B. M.; Rudraswamy, B.; Shivakumara, C.; Chakradhar, R. P. S. Spherical and Rod-Like Gd_2O_3:Eu^{3+} Nanophosphors Structural. *Bull. Mater. Sci.* **2012**, *35*, 519−527.

(13) Jia, G.; Liu, K.; Zheng, Y.; Song, Y.; Yang, M.; You, H. Highly Uniform $Gd(OH)_3$ and Gd_2O_3:Eu^{3+} Nanotubes: Facile Synthesis and Luminescence Properties. *J. Phys. Chem. C* **2009**, *113*, 6050−6055.
(14) Xu, L.; Wei, B.; An, W.; Lü, Z.; Gao, H.; Zhang, Y.; Zhang, Z. Effects of Sucrose Concentration on Morphology and Luminescence Performance Gd_2O_3:Eu Nanocrystals. *J. Alloys Compd.* **2008**, *460*, 524−528.
(15) Debasu, M. L.; Ananias, D.; Macedo, A. G.; Rocha, J.; Carlos, L. D. Emission-Decay Curves, Energy-Transfer and Effective-Refractive Index in Gd_2O_3:Eu^{3+} Nanorods. *J. Phys. Chem. C* **2011**, *115*, 15297−15303.
(16) Buijs, M.; Blasse, G. Energy Transfer between Eu^{3+} Ions in a Lattice with Two Different Crystallographic Sites: Y_2O_3:Eu^{3+}, Gd_2O_3:Eu^{3+} and Eu_2O_3. *J. Lumin.* **1987**, *37*, 9−20.
(17) García-Murillo, A.; Luyer, C. L.; Dujardin, C.; Martin, T.; Garapon, C.; Pédrini, C.; Mugnier, J. Elaboration and Scintillation Properties of Eu^{3+}-Doped Gd_2O_3 and Lu_2O_3 Sol−Gel films. *Nucl. Instrum. Methods A* **2002**, *486*, 181−185.
(18) Villabona-Leal, E. G.; Diaz-Torres, L. A.; Desirena, H.; Rodríguez-López, J. L.; Pérez, E.; Meza, O. Luminescence and Energy Transfer Properties of Eu^{3+} and Gd^{3+} in ZrO_2. *J. Lumin.* **2014**, *146*, 398−403.
(19) Benz, F.; Strunk, H. P.; Schaab, J.; Kunecke, U.; Wellmann, P. Tuning the Emission Colour by Manipulating Terbium-Terbium Interactions: Terbium Doped Aluminum Nitride as an Example System. *J. Appl. Phys.* **2013**, *114*, 073518(1−6).
(20) Chen, S.; Dierre, B.; Lee, W.; Sekiguchi, T.; Tomita, S.; Kudo, H.; Akimoto, K. Suppression of Concentration Quenching of Er-Related Luminescence in Er-doped GaN. *Appl. Phys. Lett.* **2010**, *96*, 181901(1−3).
(21) Byrd, R. H.; Hribar, M. E.; Nocedal, J. An Interior Point Algorithm for Large-Scale Nonlinear Programming. *SIAM J. Optimiz.* **1999**, *9*, 877−900.
(22) Coleman, T. F.; Li, Y. On the Convergence of Interior-Reflective Newton Methods for Nonlinear Minimization Subject to Bounds. *Math. Program.* **1994**, *67*, 189−224.
(23) Pisarski, W. A.; Zur, L.; Sołtys, M.; Pisarska, J. Terbium-Terbium Interactions in Lead Phosphate Glasses. *Appl. Phys. Lett.* **2010**, *96*, 181901(1−3).
(24) Wang, N.; Lin, H.; Li, J.; Yang, X.; Zhang, L. Photoluminescence of TiO_2:Eu Nanotubes Prepared by a Two-Step Approach. *J. Lumin.* **2007**, *122−123*, 889−891.
(25) Chih-Cheng, L.; Kuo-Min, L.; Yuan-Yao, L. Sol−Gel Synthesis and Photoluminescent Characteristics of Eu Doped Gd_2O_3 Nano-phosphors. *J. Lumin.* **2007**, *126*, 795−799.
(26) Zhanga, X.; Wanga, J.; Guoa, K.; Chen, H.; Yang, X.; Zhao, J. Synthesis and Luminescence Properties of Y_2O_3:Eu with Flower-Like Microstructure. *J. Alloys Compd.* **2012**, *517*, 149−156.
(27) Quan, Z. W.; Wang, L. S.; Lin, J. Synthesis and Characterization of Spherical ZrO_2:Eu^{3+} Phosphors by Spray Pyrolysis Process. *Mater. Res. Bull.* **2005**, *40*, 810−820.
(28) Reisfeld, R.; Eckstein, Y. Energy Transfer between Tm and Er in Borate and Phosphate Glasses. *J. Non-Cryst. Solids* **1973**, *11*, 261−284.